Journal of Intelligent & Robotic Systems (2022) 106:56
https://doi.org/10.1007/s10846-022-01755-5

SHORT PAPER

Co-design Optimization of a Novel Multi-identity Drone Helicopter (MICOPTER)

Arian Abedini[1] · **Ali Asghar Bataleblu**[1] · **Jafar Roshanian**[1]

Received: 19 February 2022 / Accepted: 9 October 2022 / Published online: 21 October 2022

Abstract
Delivery drones have always faced challenges when it comes to reliably deliver packages. This paper introduces a novel concept of a hybrid drone called "MICOPTER" to alleviate this issue. Being able to fly in three modes of aircraft, helicopter, and gyrocopter, the proposed model of the multi-identity helicopter comprises a 2DOF tilting mechanism of rotors and a folding wing system leading to better performance and controllability. To scrutinize the idea, MICOPTER is compared to other types of Unmanned Aerial Vehicles (UAVs) in terms of different performance parameters. The performance goal of the MICOPTER is the realization of a predetermined standard delivery drone mission based on Amazon Prime Air. According to the relevant literature, the corresponding conceptual design equations are formulated and the traditional matching diagram method is utilized to attain the initial design point. Afterward, a multidisciplinary-feasible design matrix is provided as well as multi-objective optimization to strive for optimal feasible configurations while maximizing cruise velocity and range. Furthermore, the configuration and performance of some of the feasible design points on the final Pareto frontier are compared with the traditional design. Finally, by simulating a typical flight profile and using robust non-linear backstepping control, the controllability of the proposed configuration is investigated. The controller performance is assessed considering its stability and tracking 8-shape trajectory. Results indicate the MICOPTER capabilities as a novel configuration in both terms of design performance and controllability.

Keywords Optimization-based design · Tiltable coaxial rotor · Folding wing · Hybrid UAV · Delivery drone · Vectorial backstepping

1 Introduction

Today, the unmanned aerial vehicle industry is rapidly developing thanks to its wide range of applications, both military and civilian [1]. Drones are broadly classified into three categories: fixed-wing, rotating-wing, and hybrid aircraft. Fixed-wing drones have a simpler structure than rotating wing ones and can fly at higher cruise speeds, at more payload capacity, and for longer times. However, some fixed wing drones may require a runway to take off and land, while those launched by hand or through a catapult mechanism usually do not require a runway [2]. Furthermore, rotating wing drones are benefited from vertical take-off and landing (VTOL), hovering flight, and high maneuverability enabling them to fly in areas with many obstacles, such as space between urban buildings. They, however, suffer from mechanical complexity, slow speed, and short flight. In addition to hovering in the vicinity alongside accomplishing a sustained cruised flight, Hybrid drones, i.e. models with fixed-wing, can take off and land vertically. This type of drone combines VTOL functionality with the standard forward propulsion of a fixed-wing drone [3]. In most hybrid VTOL drones, rotary lift propellers are normally incorporated into the wings of the aircraft, which are then tilted to forwarding flight. Fixed-wing VTOLs offer numerous benefits over traditional fixed-wing unmanned aircraft. They require much less space to launch and recover and may be carried by other vehicles such as fast boats to be used in naval warships, as they no longer require a distinctive region for take-off. They are a

✉ Arian Abedini
aryanabedini@email.kntu.ac.ir

Ali Asghar Bataleblu
ali.bataleblu@gmail.com

Jafar Roshanian
roshanian@kntu.ac.ir

[1] Department of Aerospace Engineering, K. N. Toosi University of Technology, Tehran, Islamic Republic of Iran

proper option in programs requiring aerial inspection, making the UAV covering a predetermined position for some efficient approaches to monitoring, detecting, and fighting forest fires [4].

Advances in the manufacturing, control, guidance and navigation systems, and energy storage systems have led to numerous studies for optimization and enhancement of the performance of hybrid drones, but they have not yet been fully developed. However, hybrid drones can be divided into two general categories [5]:

1.1 Convertiplane

Diverse mechanisms have been utilized to develop the convertiplane drones for the transition from vertical flight to cruise flight. The convertiplane drones can be generally categorized into 4 classes: 1) tilt-rotor, 2) tilt-wing, 3) rotor-wing, and 4) dual-systems [5]. Figure 1 depicts some of the examples of these drones.

1.2 Tail-sitter

The tail-sitter is capable of vertical take-off as well as vertical landing on its tail. The cruise flight is also achievable by tilting the entire airframe.

According to Table 1, the novel-designed UAV, MICOPTER, is categorized as a convertiplane drone. Therefore, the UAVs of this group are going to be reviewed in this paper. As presented, hybrid drones are rapidly developing. Companies such as Amazon, Google, and DHL have started substantial technical and, in some cases, coordinated public policy programs to exploit drone delivery [10].

A concrete definition of requirements, design parameters and variables, optimization objectives, and constraints is required for the integrated design optimization of mechatronic systems. Engineers from several fields must collaborate on the design approach in a multidisciplinary mechatronics design. The system is subjected to various constraints imposed by various engineering disciplines. An integrated design process is required to address the impact of these disciplines, as well as the interactions and coupling between different parameters [17]. Consequently, the present research is an attempt to implement a Multidisciplinary Design Optimization (MDO) method for the design and optimization of a hybrid drone with a new propulsion mechanism based on one of the missions defined by Amazon flying at 80 km/h at an altitude of 150 m [18]. However, for a new concept of Bi-copter such as MICOPTER, there is little relevant experience.

The most pertinent configuration in the Convertiplane category is the Mono Tiltrotor (MTR). MTR is a novel vertical takeoff and landing concept that includes a tilting coaxial proprotor, an aerodynamically actuated folding wing, and a suspended and efficient cargo handling system. The MTR, proposed by Baldwin Technology Company [19], is geared toward heavy-lift, long-range, VTOL applications, which are in high demand in today's military.

Lately, few works in coaxial rotor design have focused on multi-objective design (for both hovering and cruising states) [20], and the majority of them are predicated on parametric studies with no integrated optimization strategies [21, 22]. In addition, in other configurations such as dual systems [23] and Tail-sitters [24], design approaches using the MDO method have increased and are being developed.

(1) Bell Eagle Eye [6]

(2) DHL parcelcopter 3.0 [7]

(3) Rotor-wing UAV (THOR) [8]

(4) Arcturus JUMP 15 [9]

Fig. 1 The examples of hybrid drones. (1) Bell Eagle Eye [6]. (2) DHL parcelcopter 3.0 [7]. (3) Rotor-wing UAV (THOR) [8]. (4) Arcturus JUMP 15 [9]

Table 1 Performance record with other developed drones

Contents						
Type	Name	Years	Wing span [m]	Payload [kg]	Max speed [km/h]	Range [km]
1	Wingcopter 178 [11]	2013	1.78	6	151.2	40
	DHL Parcelcopter 4.0 [12]	2018	1.78	6	150	45
	Wingcopter 198 [13]	2021	1.98	5	144	75
2	QTW-UAS FS4 [14]	2009	1.8	5	150	20
	AVIGLE [15]	2011	2	1.5	144	45
	DHL Parcelcopter 3.0 [7]	2016	2.2	2	126	8.3
3	THOR [8]	2017	1.05	-	-	-
4	Amazon Prime Air Drone [16]	2016	0.91	2.3	80	32.2

After the MDO process, flight simulations were performed using the results obtained from the feasible design points in the Pareto frontiers. In addition to determining the controllability of the designed drone, these simulations can also justify the assumptions mentioned in the design section "A novel tilt-rotor hybrid UAV with a new propulsion mechanism to achieve maximum range and cruise efficiency". MICOPTER can perform attitude and position motions, resulting in coupled dynamics, as well as mechanically restricted systems, which do not include uncertainties/perturbations like mechanic deviations, alignments, frictions, and exact inertia in the model. As a result, in the presence of such disturbances/uncertainties, a nonlinear robust control approach based on a nominal model is required to drive the state.

Few designs of the flight control systems for tilt-rotor concepts have been investigated in the past, but they are mostly focused on quad-copters or tri-copters [25, 26] and the conceptualization of robust control schemes for flight transition [26–28]. Recently some research has been done on online identification algorithms to develop adaptive nonlinear flight control systems which could enhance the performance of the nonlinear controller algorithms in presence of different sources of uncertainties. In this way, a combination of Dynamic Programming (DP), neural networks, and reinforcement learning which is called adaptive DP have been proposed in [29, 30]. Besides, to compensate for unknown fault input according to previously recorded experiences, an Iterative learning control algorithm (ILCA) is also developed [31]. These approaches, relying on online identification, have the potential to apply to hybrid drones with novel and complex configurations.

This paper, on the other hand, focuses on bi-copter design with a new mechanism and mathematical formulation which help implement a robust control scheme. Due to the creation of the tilt mechanism with two degrees of freedom we reached a fully actuated system derived from our earlier research in which we used a robust backstepping controller to control the position and attitude of a bi-copter drone [32]. As a result, a Multi-Input Multi-Output (MIMO) vectorial backstepping control method is used to design the control inputs for the three forces and three torques in 6-DOF motions, considering the fact that the input distribution matrix is a square and nonsingular matrix that can be inverted for such a generalized vector of thrust forces and torques. Some simulation results of the proposed UAV are provided to demonstrate the decoupled control of position and attitude as well as the tracking performance of arbitrary position and attitude.

To this end, an explanation of the new concept, as well as a comparison between MICOPTER and other drones, has been presented in Section 2 to examine its advantages and disadvantages. Section 3 describes the conceptual design process. After completing the multidisciplinary design optimization in Section 4, the flight dynamic and controller design with simulation are proposed in Sections 5 and 6. The conclusions and future studies will be presented in the last section.

2 Concept Description

Performance improvement in complex missions has led to the presentation of a novel concept of hybrid drones. To explain our intentions of presenting this concept, a comprehensive classification of previously realized drones based on their flight mechanism should be first provided. According to the latest analysis, hybrid drones can be classified into three types:

- The first type, including the wing and the tilting mechanism of the rotors.
- The second type, which has no wings and is similar to helicopters.
- The third type, including the wings but without the mechanism of tilting the rotors [33].

The purpose of presenting this new conceptual design includes the wing and the mechanism of tilting the rotors (the first type). Folding wings changes drones to helicopter configuration (the second type) that can perform more complex missions. This concept is illustrated in Fig. 2.

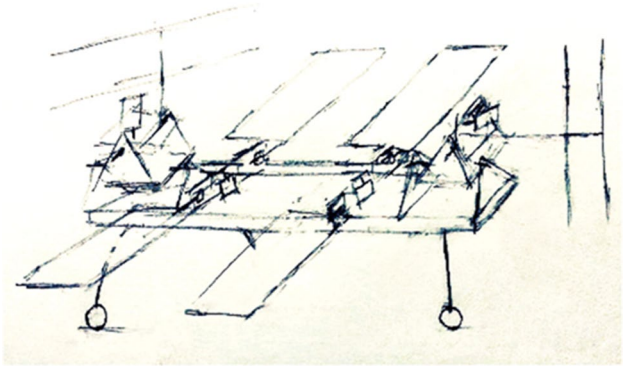

Fig. 2 A Drawing of the Intended Concept

2.1 Configuration

The idea for the hybrid drone originated from a Bi-copter [32]. A fixed-wing system was also added to the mechanism allowing for back and forth tilting of the engines to improve the performance of the helicopter. Now the question is what kind of wings to consider. According to [34], for the same wing area, better performance can be achieved by having two wings. Therefore, a special mechanism was designed for folding two wings.

2.2 Mechanism of Motion

This unmanned vehicle uses two 2DOF tiltable motors on one axis. The required thrust and lift power are provided by transmitting the motor power to the propellers (in airplane mode, the lift force will be borne by the wings) in such a way that one propeller operates clockwise while the other acts counterclockwise. Balance, control, and stability can be achieved by changing speeds, tilting angles, and pitch blades. By replacing the coaxial system [35] for each rotor, there will be no gyroscopic effect on the rotors, neither roll nor yaw channel couplings.

2.3 Advantages and Disadvantages

Advantages of the designed UAV over other hybrid UAVs:

- It has folding wings which can save engine power in vertical flight.
- Due to the location of the rotors in the longitudinal axis of the drone, there is no need to control the surfaces.
- Ability to fly in gyrocopter mode and save energy.
- Maintains altitude in the transition mode between the two helicopter modes to the aircraft

The changes in UAV configuration are depicted in Fig. 3.

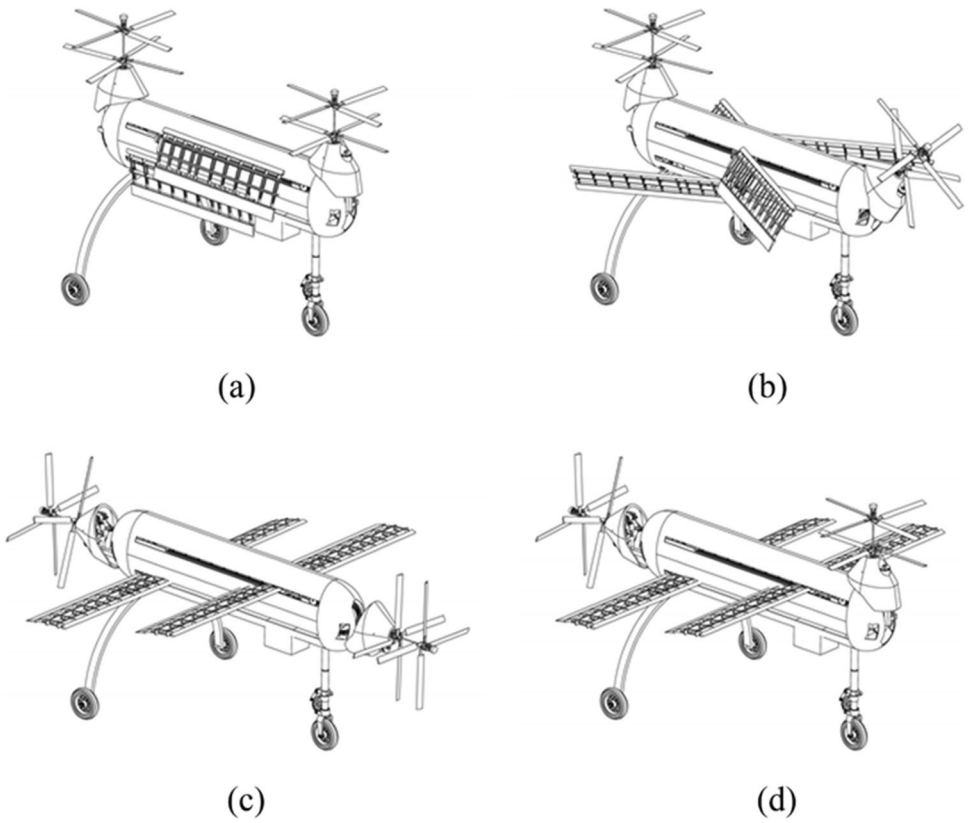

Fig. 3 MICOPTER configurations, **a** A perspective view of the MICOPTER in helicopter mode, **b** The transition mode, **c** The airplane mode, **d** Finally, the gyrocopter mode

Table 2 Performance record with other developed drones

Feature	Configurations						
	CMR	CAR	TR	4R	6R	8R	MI
Ease of Development	1	2	3	5	4	3	4
Cost of Development	2	4	4	4	3	2	4
Ease of Control	1	2	2	4	3	2	3
Mechanical Simplicity	1	2	3	4	3	2	3
Aerodynamic complexity	2	3	3	3	3	3	3
Maneuverability	2	4	3	4	4	4	4
Miniaturization	2	4	3	5	4	3	3
Survivability	3	3	3	3	3	3	3
Low speed flight	3	3	3	3	3	3	5
High speed flight	2	2	2	2	2	2	5
Power efficiency	5	5	4	4	2	2	5
Payload capability	2	2	3	4	5	5	4
Modularity	2	2	3	4	3	3	3
TOTAL	28	40	39	49	43	37	49

To evaluate the value of UAV research and development, effective factors were taken into account and the new hybrid UAV was compared with the other UAVs. A grading system was utilized which ranged between 1 and 5 in which scores of 1, 2, 3, 4, and 5 stand for fair, average, good, very good, and excellent, respectively. As known, the multirotor vehicle possesses numerous variants defined by the number of rotors. Thus, four, six, and eight rotor variants were taken into account for this comparison in which 4R, 6R, and 8R represent Quadrotor, Hexacopter, and Octocopter, respectively [36]. CMR (Conventional main rotor), CAR (Coaxial rotors), TR (Tandem rotor), and MI (MICOPTER). The details can be found in Table 2.

The results of the above table indicated that the MICOPTER can acquire an excellent score in the maximum and minimum speed parameters due to the installation of a 2DOF mechanism for the rotors, the wing folding mechanism, and the ability to change the configuration to three modes: aircraft, helicopter, and gyroscope. Furthermore, it achieves the best performance in optimal energy consumption, which outperforms the other configurations and is equal to the quadrotor, thanks to the change of configuration to gyroscope mode (which reduces the front engine speed by half).

3 Conceptual Design

There is no definitive method for designing hybrid drones. Regarding their combined configuration, a design method should be sought. Following the conceptual and initial design method developed for Tilt Rotor by [37], articles have employed this method. For instance, a study was carried out in [38], which involved a Multidisciplinary design optimization using the open-source tools linking. This method is also applied in this research.

3.1 Mission Specifications

Ordinary mission profiles of the UAV are defined through six following steps:

- Take-off (vertical or fixed-wing).
- Hovering.
- The transition from helicopter to fixed-wing flight modes.
- Cruise like a fixed-wing UAV.
- The transition from fixed-wing to helicopter flight modes.
- Landing.

The mentioned task profile determines the primary set of duties. Other tasks (e.g., entering collapsed buildings to find victims) were not considered. Moreover, the mission profile does not encompass several transition operations, as they are apparent and depend on the purpose(s) of the plane [37]. The posted performance goals of Amazon top Air were employed by the standard shipping drone task. The drone must fly at 80 km/h at an altitude of 150 m (400 feet) (Amazon, undated). The mission characteristics are summarized in Table 3.

Table 3 Required Mission Specifications

Parameter	Value	Parameter	Value
Overall Cruise Range [km]	40	Fixed-wing rate of climb [m/s]	5
Cruise Altitude [km]	0.15	Runway length for take-off [m]	30
Maximum Speed [km/h]	80	Hovering altitude [km]	0.15
Stall Speed [m/s]	13	Helicopter rate of climb [m/s]	8
Payload weight [kg]	2.3	Hover ceiling altitude [km]	0.5

3.2 Configuration Selection

As described in the Concept description section, a combination of a winged Bi-copter was used in which two motors can tilt in 2DOF. The rotors employed a coaxial system and the motors are tilted forward and backward. The pitch of the rear blades was reversed. In the same way, symmetrical blades were used. Most products on the market use a dual system configuration. The quadrotor attached to the aircraft frame was the least complicated solution. Adding extra structures and engines can increase body drag force while imposing dead weight on cruise flight, which is not an optimal choice for a high endurance mission. Thus, the developed configuration is a better candidate for long end missions. It can operate with fewer engine numbers in addition to being cost-effective.

3.3 Propulsion

The choice of propulsion is the most essential part to exploit the most out of the aircraft and reach the desired range. Due to using a coaxial system for the rotor during cruise flight, there will be no significant unbalanced distribution of load on the front and rear engines. When hovering, both engines share a common load. This means that extra power and thrust will not be used for separate engines like most Tricopters. The design is more efficient due to reducing energy consumption.

3.4 Weight Estimation

According to [10] who analyzed the performance of delivery UAVs and based on Table 4 given by this reference, considering the average between the first and second package numbers, the weight of the UAV was estimated at 11 kg.

3.5 Initial Sizing

This stage well estimated the two driving elements for any design wing loading and power loading. Suitable relations were derived for the transition, hover, and climb stages for the tiltrotor sizing to account for disc loading. As a rough estimate is preferred at this point, a design space is created for linear programming based on [37]. With the aid of the matching diagram in Fig. 4, the design parameters can be selected for the MICOPTER. Upon selection of the design parameters, the aircraft power, wing area, and rotor diameter are determined based on the estimated UAV weight. Table 5 presents the results of the conceptual design:

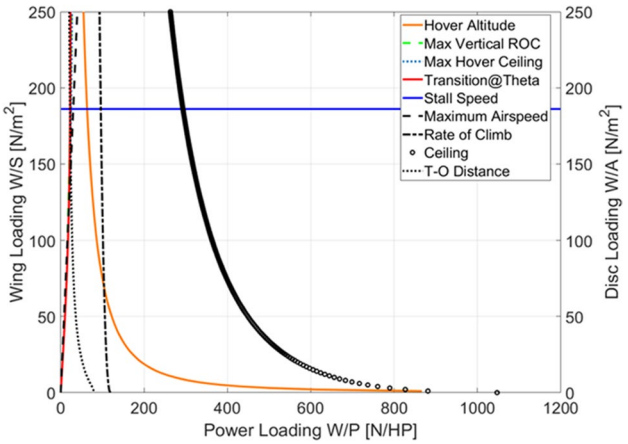

Fig. 4 Matching Diagram for Hybrid UAV

4 Multidisciplinary Design Optimization

An efficient strategy is presented in the current research to optimize the conceptual design of a Novel Multi-Identity Drone Helicopter by MDO methodology. The MICOPTER modeling is organized as a multi-objective design optimization problem for maximizing the cruise speed and range. The NSGA-II algorithm was utilized for the optimization which was aimed to design a geometry and propulsion device to achieve maximum range and maximal cruise efficiency.

Diverse methods can be used to deterministically find the proper MDO method for this project. Herein, a Multidisciplinary feasible (MDF) [39] process was implemented for designing a Novel Multi-Identity Drone Helicopter in the cruise phase for maximizing the cruise speed and

Table 4 Requirements for Multi-Stop Delivery as an Example

Number of Packages	Payload Mass (kg)	Range (km)	Drone Mass (kg)
1	2.3	32.2	7.5
2	4.6	40.2	14.5
3	6.9	48.3	23.1
4	9.2	56.3	33.8

Table 5 Results of the MICOPTER Conceptual Design Phase

Parameter	Value	Parameter	Value
Take-off mass [kg]	13.3	Empty weight [kg]	11
Wing loading [N\m^2]	179.1	Power loading [N\hp]	22.59
Wing area [m^2]	0.73	Wing aspect ratio [-]	6.7
Rotor disc loading [N\m^2]	178	Maximum take-off power [hp]	5.7

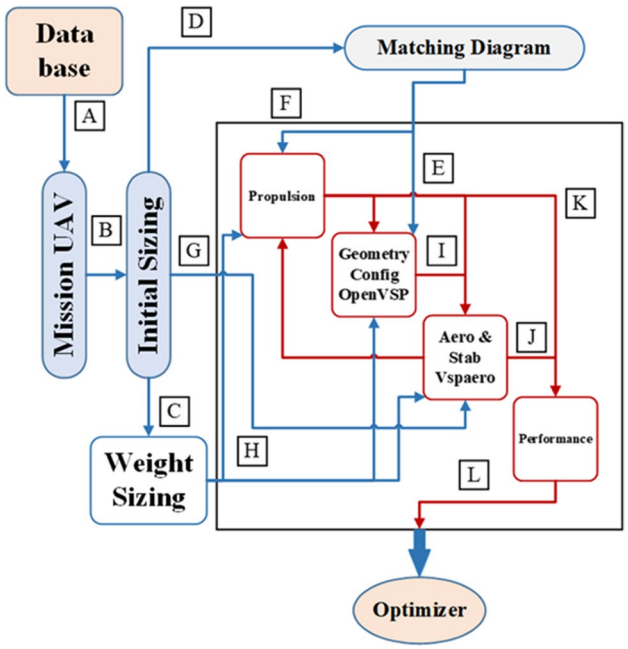

Fig. 5 Multidisciplinary Design matrix

flight range using four disciplines. Geometry of Configuration, aerodynamic and stability, propulsion selection, and performance are the disciplines that were coupled in this project. Figure 5 demonstrates the correlation between disciplines during MDF analysis.

In the design matrix of this drone, the inputs and outputs related to each subject are specified in Latin letters as follows:

A. Hybrid UAV Database	G. Dimensions required after initial drone sizing
B. Mission-appropriate hybrid drones	H. Total mass
C. Estimate the initial weight	I. Calculated parameters of geometry
D. Dimensions required	J. Aerodynamic coefficients
E. Ratio of weight to wing area	K. Engine specifications, engine power
F. Ratio of weight to engine power	L. Cruise velocity and range of the UAV

4.1 Disciplines Definition

4.1.1 Geometry of Configuration

In this regard, the UAV was modeled by OpenVSP software [40]. This is an open-source software published by NASA in 2012 which:

- allows the creation and variation of any conceptual aircraft configuration based on its set of fully parameterized aircraft components.

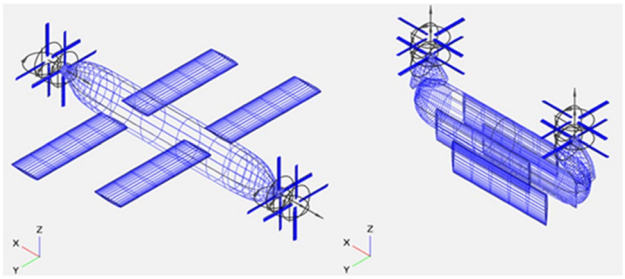

Fig. 6 Geometric model of MICOPTER in the OpenVSP Software

- has fast aerodynamic calculation capabilities.
- can run any task from the command line, allowing fully automated design and optimization.

The geometry of the aircraft is also generated by OpenVSP, which is the object of the aerodynamic computations. Then, OpenVSP processes are automated using MATLAB [41]. Based on the results of the conceptual design in Table 5 in two modes: airplane and helicopter as depicted in Fig. 6.

According to the configuration definition, the parts related to the 2DOF mechanism, and the stepper motor placement are fixed; only the part between the two red lines (shown in Fig. 7) changes based on the smaller or larger wingspan.

4.1.2 Aerodynamic and Stability

The aerodynamic module "VSPAero" which is integrated into OpenVSP, is used to compute aerodynamic coefficients. The module employs a linear VLM method that calculates induced drag using the Trefftzplane approach. It is a quick, linear method for evaluating the aerodynamic model at the

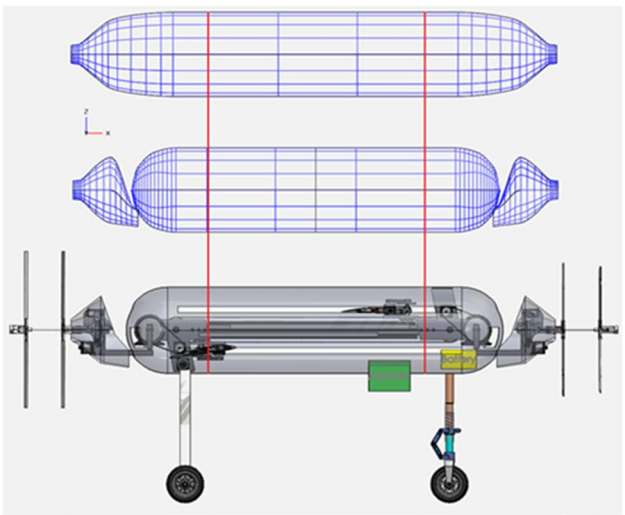

Fig. 7 Geometric model of MICOPTER changes with increasing and decreasing wing size

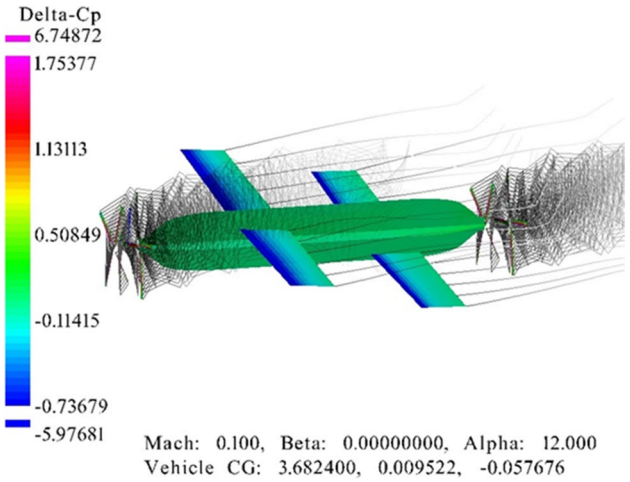

Fig. 8 The pressure distribution contour under climbing flight conditions

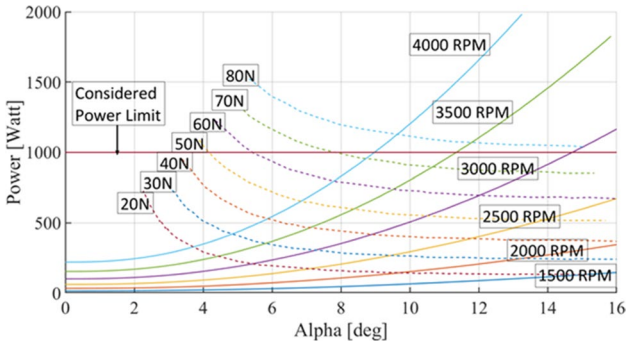

Fig. 10 The constant RPM lines (solid lines) and constant thrust lines (dash lines)

conceptual level. In order to conduct a comparison study to investigate the accuracy of this module researchers compared VSPAero with Star CCM + (RANS CFD), FlightStream (surface vorticity solver), and wind tunnel aerodynamic results, which showed higher efficiency of the VSPAero [42]. In this case, the simulation was conducted in the VSPAero using the Vortex Lattice method [43]. In a flight condition (Fig. 8), more accurate aerodynamic coefficients and stability derivatives were obtained as the propulsion system was fully modeled. The initial estimation of aircraft performance was first analyzed by XFLR5 [44] focusing entirely on airfoil selection and obtaining preliminary, yet knowledgeable estimates of static stability parameters. Wing planform was initially estimated through the use of NACA airfoils on the angle of attack at peak *Cl*/*Cd* values running at cruising altitude and velocity, resulting in the selection of NACA 4412 airfoil.

4.1.3 Propulsion Selection

For selecting the propulsion according to the special design of the MICOPTER, during the transfer, the rear engine turns in the back direction and must be the push power in some way; therefore, symmetrical airfoil blades are required. According to [45], NACA 0017 airfoil is suitable for VTOL UAVs.

Based on the results of the initial estimates, the standard of a 325 mm blade was selected (see Fig. 9). Take the blade's spinning rate of 3000 RPM, Mach number of 0.31 at the tip of the blade while the Reynolds number is 241,000. The rotor blade used NACA 0017 airfoil based on the XFLR5 airfoil analysis; the mentioned airfoil stalls at an attack angle of 14°. This condition declines the maximum RPM of the rotor to 3100 RPM. Using Qprop software [46], the number of blades per rotor was checked according to the initial weight estimate of 17 kg (With a payload of 6 kg) and based on the coaxial rotors. Four blades per rotor were then achieved. At 14 degrees of pitch angle, the maximum rotor generated thrust is ~ 70 N or 15.7 lbf. Higher thrust levels will lead to blade stalling, which is depicted in Fig. 10.

The next step is to determine the distance between the two rotors. According to [47], for the 4-blade coaxial rotor, if the distance between the two rotors is 0.25 of the rotor diameter, the maximum lifting force will be achieved.

Fig. 9 325 mm length of a helicopter rotor blade

a) **Motor selection**

Hacker A60-20 M brushless motor was selected for this UAV which has greater power and torque in comparison with brushed DC motors. This motor possesses maximum power of 2,200 W at the rate of 170 kV [45]. Despite its low RPM, the 12 poles confirm the high torque of this motor, making it a suitable option for MICOPTER.

b) **Battery selection**

Regarding modern trends of electric propulsion in aviation, Lithium-Ion battery packs prove to be the best choice in terms of electricity density as they keep higher amperage in comparison with their Lithium polymer counterparts. Lithium-Ion battery packs, however, suffer from limited current discharge [48]. Therefore, two 10S lithium polymer batteries were used due to the implementation of two high-current brushless motors, as well as five stepper motors and two servo motors.

4.1.4 Performance

Range and flight continuity are the most important features of a drone. Extension of the range and continuity of flight is desirable due to the need to establish other restrictions. The range can be obtained by the following equations [49]:

$$R = \frac{1}{g}\eta_p \eta_{tr} \eta_{batt} E_{spec} \frac{W_{batt}}{W_{to}} \sqrt{\frac{1}{4C_{D0}K}} \tag{1}$$

$$E_{spec} = \frac{VC \times 3600}{m_{batt}} \tag{2}$$

where η_p, η_{tr}, and η_{batt} are propeller efficiency, transmission efficiency, and battery efficiency, respectively. V refers to the voltage and C is the capacity of the battery used in the MICOPTER. $K = 1/\pi eAR$ that e and AR are Oswald's efficiency factor and the aspect ratio, respectively. g denotes gravitational acceleration and C_{D0} is zero-lift drag coefficient. W_{to} represents total weight, whereas W_{batt} denotes battery weight.

Cruise flight is generally performed in steady-state flight mode at a constant speed; whose effect on performance can be determined by efficiency and battery consumption. Cruise speed is obtained from the following equation:

$$V_{Cruise} = \sqrt{\frac{2\left(W_{to} - \left(T_{thrust,1}\right)\sin\left(\beta_1\right) - \left(T_{thrust,2}\right)\sin\left(\beta_2\right)\right)}{\rho.s\sqrt{\frac{C_{D0}}{K}}}} \tag{3}$$

In which β_1 and β_2 are the tilted angles, ρ denotes the density, $T_{thrust,1}$ and $T_{thrust,2}$ are the rotor thrust, and s refers to the wing area.

4.2 Optimization Process

4.2.1 Optimization Algorithm (NSGA-II)

Multi-objective evolutionary optimization techniques such as Non-dominated Sorting Genetic Algorithm-II (NSGA-II) have been extensively employed for balancing competing objectives. Details on NSGA-II can be found in [50]. In the present study, the simulation codes were run in MATLAB. The corresponding Pareto solutions are obtained after 20 generations with population size 50, crossover operator ratio 0.8, and Mutation operator Scale = 0.1, Shrink = 0.5.

4.2.2 Objective Function

The conceptual design of the MICOPTER was optimized through a multi-objective problem. The cruise and range were maximized to assess the overall performance of the system. Two objectives should be coupled (e.g., by Pareto-Frontier).

Table 6 Design Variables

Design Variable		Units	Lower Bound	Upper Bound
Front & rear wings	Incidence angle	[deg]	-5	5
	Position in the direction of z	[m]	0.1	0.135
	Sweep angle	[deg]	0	5
	Dihedral angle	[deg]	0	2
	Root Chord	[m]	0.15	0.3
	Wingspan	[m]	0.5	2

4.2.3 Design Variables

Ten design variables including wing and fuselage dimensions were chosen whose bounds are listed in Table 6.

4.2.4 Design Constraints

Here, design constraints relied on dimensional and stability requirements analysis that are bounded on the basis of the values expressed by [51] are listed in Table 7.

4.3 Results

The optimum results and related design variables are shown in Table 8. At the end of the optimization process, all constraints were satisfied. The resulted Pareto frontier is depicted in Fig. 11. The configuration and objectives of three selected points were compared as presented in Fig. 12 and Table 8. The feasible design points in the Pareto frontiers confirmed that the MICOPTER can fulfill the mission goals as well as having the ability to carry payloads up to 6 kg in different velocities and ranges with minimum changes in the configuration.

This paper presents a novel configuration of a hybrid drone that fulfills the Amazon Prime Air standard delivery drone requirements. This configuration not only satisfies the required specifications but also provides better performance characteristics. A technique was

Table 7 Design Constraints

Disciplines	Constraint	Units
Geometry of Configuration	$5 < AR < 7$	-
Aerodynamic and Stability	$Cm_{\alpha} < 0$	-
Propulsion power efficiency	$Power_{Front\ rotors} < 1700$	[w]
	$Power_{Rear\ rotors} < 1700$	[w]
Performance	$50 <$ Cruise velocity < 150	[km/h]
	Range > 50	[km]

Table 8 Design Variables and Objective Functions of Selected Points

Design Variable		Unit	Payload [kg]					
			2			6		
			Max. Range	Selected Point	Max. Velocity	Max. Range	Selected Point	Max. Velocity
Front wing	Incidence angle	[deg]	1.87	2.37	2.55	-1.3	-0.57	1.6
	Position in z direction	[mm]	129	128	129	131	131	133
	Sweep angle	[deg]	1.2	2.3	3.45	3.85	1.2	0.43
	Dihedral angle	[deg]	0.4	0.3	0.25	0.8	1.5	1.2
	Root Chord	[mm]	205	171	197	238	190	194
	Wingspan	[mm]	1025	601	689	1247	893	559
Rear wing	Incidence angle	[deg]	1.1	1.1	-1.3	-2.9	-3.68	-3.37
	Position in z direction	[mm]	-129	-133	-128	-110	-105	-101
	Sweep angle	[deg]	3.6	4	3.75	1.76	3	3
	Dihedral angle	[deg]	1	1	1	1.58	1.2	1.58
	Root Chord	[mm]	205	171	197	238	190	194
	Wingspan	[mm]	1025	601	689	1247	893	559
Optimal objective function	Cruise velocity	[km/h]	63.3	81	144.6	64.9	81.4	147.4
	Range	[km]	111.7	92.6	50.3	100	89	50

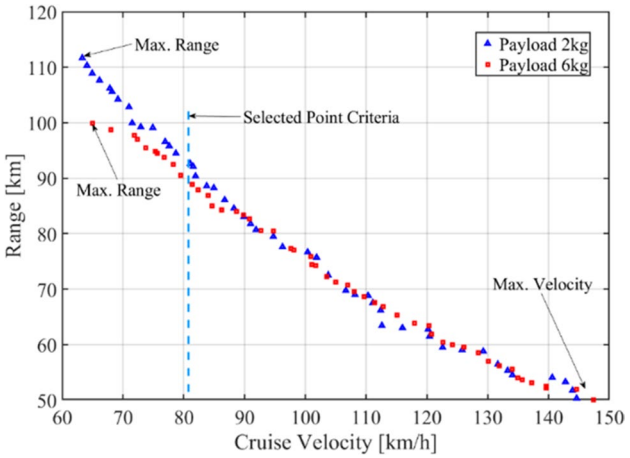

Fig. 11 The resulted Pareto front for two objective functions

proposed to review the traditional method of initial aircraft evaluations, which is based solely on statistical data and regression of other aircraft, and finally proposed an MDO-based method that uses low-order aerodynamics, weight distribution, and structural computational analysis. This method was able to optimize the aircraft, as mentioned in Section 3 (Table 5). As a result, the dimensions of the drone have been optimized, which has resulted in fewer drag forces, and therefore increased performance (see Fig. 12). Due to the design constraints (Table 7), selected motors were able to reach the required power (3400 watts, equivalent to 4.55 hp), which is almost 20% less than the calculated power from the traditional design aspect (5.7 hp). This method allows the designer to evaluate the operational characteristics of the aircraft such as direct operating costs (DOC) and the sensitivity level of perceived effective design variables from initial design steps.

5 Dynamic Model

With only four input controls, the Bi-copter has six degrees of freedom. It's a severely under-actuated system. The control amount is coupled, which belongs

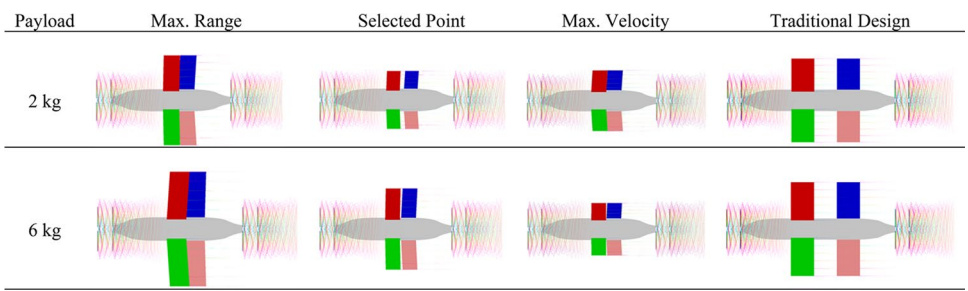

Fig. 12 Dimensional changes in the selected points compared with the traditional aircraft design

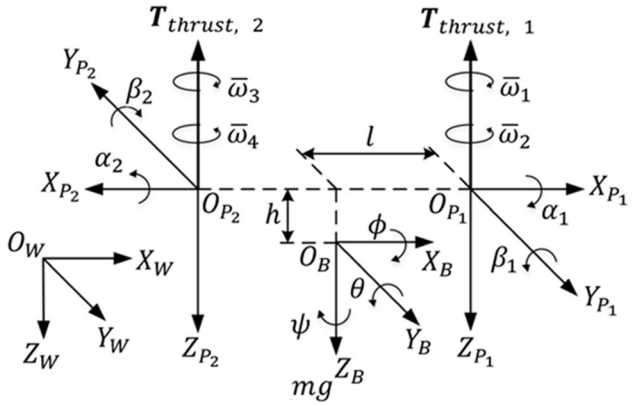

Fig. 13 Coordinate systems related to the MICOPTER

to the nonlinear system [32]. The MICOPTER, on the other hand, can be a fully actuated system due to the installation of a 2DOF mechanism for the rotors, which is detailed in this section. Figure 13 demonstrates the coordinate system for the MICOPTER with 2DOF tiltable coaxial rotors. A 3D model of the Max range selected point with 6 kg payload is depicted in Fig. 14.

The world frame $\mathcal{F}_w$ is defined relative to the origin O_w following the right-hand coordinate system with the axes $\{X_w, Y_w, Z_w\}$. The body frame $\mathcal{F}_B$ definition is related to the origin O_B fixed to its center of mass with the axes $\{X_B, Y_B, Z_B\}$. $\mathcal{F}_{P1}$ refers to the first tiltable coaxial rotor coordinate frame with respect to the origin O_{P1} with the axes of $\{X_{P1}, Y_{P1}, Z_{P1}\}$, whereas the second one, $\mathcal{F}_{P2}$ is defined relative to the origin O_{P2} with the axes $\{X_{P2}, Y_{P2}, Z_{P2}\}$ [52].

To simplify the process, the coordinate frame of the i-th ($i=1,2$) tiltable coaxial rotor is unified to$\mathcal{F}_{Pi}$. The rotation angles around theX_B, Y_B and Z_B axis in $\mathcal{F}_B$ are defined as (ϕ, θ, ψ), whereas the tilt angles around the Y_{Pi} and X_{Pi} axis in $\mathcal{F}_{Pi}$ are denoted by (β_i,α_i). The tilt angle of α_i ranges in $[-\frac{\pi}{2}, \frac{\pi}{2}]$, whereas the tilt angle of β_i varies in $[-\frac{\pi}{2}, 0]$.

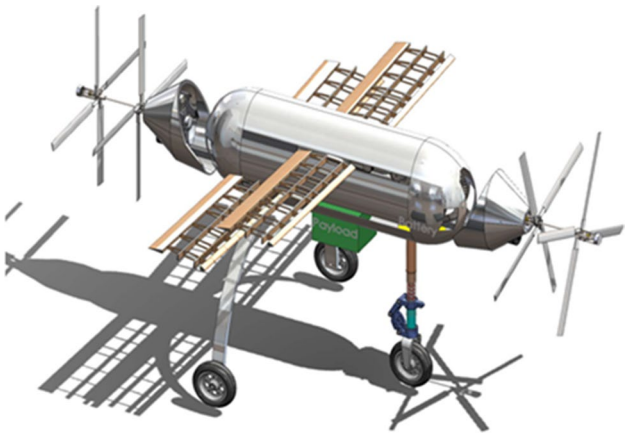

Fig. 14 3D model of the Max range selected point with 6 kg payload

The rotation matrix ${}^{w}\boldsymbol{R}_{\mathrm{B}} = \boldsymbol{R}_Z(\psi)\boldsymbol{R}_Y(\theta)\boldsymbol{R}_X(\phi)$ refers to the rotation from $\mathcal{F}_B$ to $\mathcal{F}_W$, where $\boldsymbol{R}_Z$, $\boldsymbol{R}_Y$ and $\boldsymbol{R}_X$ show the rotations around the Z_B, Y_B and X_B axis, respectively. Moreover, ${}^{B}\boldsymbol{R}_{\mathrm{Pi}} = \boldsymbol{R}_Z((i-1)\pi)\boldsymbol{R}_Y(\beta_i)\boldsymbol{R}_X(\alpha_i)$ denotes the rotation matrix from F_{Pi} to $\mathcal{F}_B$, in where $\boldsymbol{R}_Z$, $\boldsymbol{R}_Y$ and $\boldsymbol{R}_X$ stand for the rotations around the Z_{Pi}, Y_{Pi} and X_{Pi} axis, respectively. The length l refers to the distance between the origin of each coaxial rotor O_{Pi} and the axis Z_B of the MICOPTER, while the height h stands for the distance between the origin of O_{Pi} and O_B in Z_B direction. The position vector $\boldsymbol{O}_{Pi}$ of the i-th tiltable coaxial rotor in $\mathcal{F}_B$ is represented by ${}^{B}\boldsymbol{O}_{Pi} = \boldsymbol{R}_Z((i-1)\pi)[l\ 0\ h]^T$. According to Fig. 13, $\overline{\omega}_1$, $\overline{\omega}_2$, $\overline{\omega}_3$ and $\overline{\omega}_4$ indicate the rotation speed of the brushless motors in the corresponding coaxial rotor. Therefore, the anti-torque $\tau_{drag,i}$ of the i-th coaxial rotor could be expressed by:

$$\begin{cases} \boldsymbol{\tau}_{drag,1} = \left[0\ 0\ k_m\left(\omega_2^2 - \omega_1^2\right)\right]^T \\ \boldsymbol{\tau}_{drag,2} = \left[0\ 0\ k_m\left(\omega_3^2 - \omega_4^2\right)\right]^T \end{cases} \tag{4}$$

where k_m is the propeller drag coefficient and $k_m > 0$. Furthermore, the total output thrust $T_{thrust,i}$ of each coaxial rotor is given by:

$$\begin{cases} \boldsymbol{T}_{thrust,1} = \left[0\ 0\ -k_f\left(\omega_1^2 + \omega_2^2\right)\right]^T \\ \boldsymbol{T}_{thrust,2} = \left[0\ 0\ -k_f\left(\omega_3^2 + \omega_4^2\right)\right]^T \end{cases} \tag{5}$$

In which k_f denotes the propeller thrust coefficient and $k_f > 0$. To simplify the control model, the anti-torque $\boldsymbol{\tau}_{drag,i}$ of the i-th tiltable coaxial rotor was removed by setting $\overline{\omega}_1 = \overline{\omega}_2 = \omega_1$, $\overline{\omega}_3 = \overline{\omega}_4 = \omega_2$, where ω_1 and ω_2 stand for new rotation speeds of the brushless motors in each tiltable coaxial rotor. Thus, the anti-torque $\boldsymbol{\tau}_{drag}$ can be determined by:

$$\boldsymbol{\tau}_{drag} = \boldsymbol{\tau}_{drag,1} + \boldsymbol{\tau}_{drag,2} = 0 \tag{6}$$

Furthermore, the gyro moment effect of the tiltable coaxial rotors is negligible by un-modeling the tilt angular velocities and their corresponding accelerations.

5.1 Dynamical equations in rotation

Thus, $\boldsymbol{\omega}^B \triangleq \left[\dot{\phi}\ \dot{\theta}\ \dot{\psi}\right]^{\mathrm{T}}$ shows the angular velocity of the MICOPTER within the body coordinate system. Considering Newton–Euler's law, ω^B is subject to:

$$\boldsymbol{I}_B\dot{\boldsymbol{\omega}}^B + \boldsymbol{\omega}^B \times \boldsymbol{I}_B\boldsymbol{\omega}^B = \boldsymbol{\tau}^B + \boldsymbol{\tau}_{ext} \tag{7}$$

where $\boldsymbol{I}_B$=diag(I_{Bxx}, I_{Byy}, I_{Bzz}) denotes the symmetric and positive definite inertia matrix of the body, $\boldsymbol{\tau}^B$ refers to the input torque, and $\boldsymbol{\tau}_{ext}$ shows the unmodeled disturbance. Neglecting the effect of the unmodeled disturbance, $\boldsymbol{\tau}_{ext} = 0$, while the input torque $\boldsymbol{\tau}^B$ can be written by:

$$\boldsymbol{\tau}^B = \boldsymbol{\tau}_{thrust} + \boldsymbol{\tau}_{wing} + \boldsymbol{\tau}_{drag} = \boldsymbol{\tau}_{thrust} + \boldsymbol{\tau}_{wing} \tag{8}$$

In which the moment $\boldsymbol{\tau}_{thrust}$ due to the thrusts induced by the tiltable coaxial rotors will be:

$$\boldsymbol{\tau}_{thrust} = \sum_{i=1}^{2} ({}^{B}\boldsymbol{O}_{P_i} \times {}^{B}\boldsymbol{R}_{P_i} \boldsymbol{T}_{thrust,i}) \tag{9}$$

And the moment $\boldsymbol{\tau}_{wing}$ due to the lifts generated by the wings can be expressed by:

$$\begin{gathered} \boldsymbol{\tau}_{wing} = \begin{bmatrix} \bar{L} \, M \, N \end{bmatrix}^{T} \\ \bar{L} = 0.5\rho V^2 SbC_l, \; M = 0.5\rho V^2 Sc_A C_m, \; N = 0.5\rho V^2 SbC_n \end{gathered} \tag{10}$$

where $\bar{L}$, M and N show the roll moment, pitch moment, and yaw moment of the MICOPTER, respectively, ρ denotes the density, V refers to the flight velocity, S is the wing area, b denotes the wingspan, and c_A represents the mean aerodynamic chord.

By denoting resultant input torque as $\boldsymbol{\tau}_{input} = [\tau_x^{thrust} \; \tau_y^{thrust} \; \tau_z^{thrust}]^T$ the dynamical model of the rotational motion of the MICOPTER can be presented by:

$$\begin{bmatrix} \ddot{\phi} \\ \ddot{\theta} \\ \ddot{\psi} \end{bmatrix} = \begin{bmatrix} \dot{\theta}\dot{\psi}\left(\frac{I_{Byy}-I_{Bzz}}{I_{Bxx}}\right) + \frac{1}{I_{Bxx}}\tau_x^B \\ \dot{\phi}\dot{\psi}\left(\frac{I_{Bzz}-I_{Bxx}}{I_{yy}}\right) + \frac{1}{I_{Byy}}\tau_y^B \\ \dot{\phi}\dot{\theta}\left(\frac{I_{Bxx}-I_{Byy}}{I_{Bzz}}\right) + \frac{1}{I_{Bzz}}\tau_z^B \end{bmatrix} \tag{11}$$

5.2 Dynamical Equations in Translation

According to the Newton equation of motion, the MICOPTER body position $\boldsymbol{P}=[x \; y \; z]^{\mathrm{T}}$ in the world coordinate system is exposed to:

$$m\ddot{\boldsymbol{P}} = m\begin{bmatrix} 0 \\ 0 \\ g \end{bmatrix} + {}^{w}\boldsymbol{R}_B \sum_{i=1}^{2} {}^{B}\boldsymbol{R}_{pi}\boldsymbol{T}_{thrust,i} + \boldsymbol{f}_{wing} + \boldsymbol{f}_{ext} \tag{12}$$

In which $\boldsymbol{f}_{ext}$ encompasses disturbances and unmodeled factors and g shows the gravity constant. According to the relationship between body coordinate frame and wind coordinate, the forces $\boldsymbol{f}_{wing}$ due to the lifts generated by the wings is:

$$\begin{gathered} \boldsymbol{f}_{wing} = \begin{bmatrix} -D\cos\alpha\cos\beta - Y\cos\alpha\sin\beta + L\sin\alpha \\ -D\sin\beta + Y\cos\beta \\ -D\sin\alpha\cos\beta - Y\sin\alpha\sin\beta - L\cos\alpha \end{bmatrix} \\ L = 0.5\rho V^2 SbC_L, \; D = 0.5\rho V^2 SC_D, \; Y = 0.5\rho V^2 SC_Y \end{gathered} \tag{13}$$

where L, D, and Y are the lift, drag, and side force of the MICOPTER, respectively. Neglecting the effect of friction, $\boldsymbol{f}_{ext}$ could be adjusted to 0. Denoting the input thrust $\boldsymbol{f}_B$ in $\mathcal{F}_{\mathrm{B}}$ as:

$$\boldsymbol{f}^B = \sum_{i=1}^{2} ({}^{B}\boldsymbol{R}_{P_i}\boldsymbol{T}_{thrust,i}) + \boldsymbol{f}_{wing} = [F_x^B \; F_y^B \; F_z^B]^T \tag{14}$$

The dynamical model of the translational motion of the MICOPTER will be:

$$\begin{bmatrix} \ddot{x} \\ \ddot{y} \\ \ddot{z} \end{bmatrix} = \begin{bmatrix} 0 \\ 0 \\ g \end{bmatrix} + \frac{1}{m}{}^{w}\boldsymbol{R}_B \begin{bmatrix} F_x^B \\ F_y^B \\ F_z^B \end{bmatrix} \tag{15}$$

5.3 Dynamical Equations of the System

Combining the Eqs. (11) and (15), the matrix form of the dynamical model of the system will become:

$$\ddot{\boldsymbol{X}} = \boldsymbol{f}(\dot{\boldsymbol{X}}) + \boldsymbol{g}(\boldsymbol{x})(\boldsymbol{U} + \boldsymbol{w}) \tag{16}$$

In the above equation, $\boldsymbol{X} = [x \; y \; z \; \phi \; \theta \; \psi]^T$ shows a generalized coordinate vector relative to the MICOPTER, $\boldsymbol{U}=[f^B \; \tau_{thrust}]^T$ represents a vector of the thrust forces and torques of the coaxial rotors expressed in the body coordinate system on X_B, Y_B and Z_B axis and $\boldsymbol{w} = [\boldsymbol{f}_{wing} \; \boldsymbol{\tau}_{wing}]^T$. $\boldsymbol{f}(\dot{\boldsymbol{X}})$ and $\boldsymbol{g}(\boldsymbol{X})$ can be represented by:

$$\boldsymbol{f}(\dot{\boldsymbol{x}}) = \begin{bmatrix} 0 \\ 0 \\ g \\ \dot{\theta}\dot{\psi}\left(\frac{I_{Byy}-I_{Bzz}}{I_{Bxx}}\right) \\ \dot{\phi}\dot{\psi}\left(\frac{I_{Bzz}-I_{Bxx}}{I_{yy}}\right) \\ \dot{\phi}\dot{\theta}\left(\frac{I_{Bxx}-I_{Byy}}{I_{Bzz}}\right) \end{bmatrix} \tag{17}$$

$$\boldsymbol{g}(\boldsymbol{x}) = \begin{bmatrix} \frac{1}{m}{}^{w}\boldsymbol{R}_B & 0 \\ 0 & \boldsymbol{M}_{IB}^{-1} \end{bmatrix} \tag{18}$$

In which $\boldsymbol{g}(\boldsymbol{X}) \in \mathbb{R}^{6\times6}$ and $\boldsymbol{M}_{I_B} = \mathrm{diag}(I_{Bxx}, I_{Byy}, I_{Bzz})$. It is proven that $\boldsymbol{g}^{-1}(\boldsymbol{X})$ and it can be obtained as:

$$\boldsymbol{g}^{-1}(\boldsymbol{X}) = \begin{bmatrix} m{}^{w}\boldsymbol{R}_B^T & 0 \\ 0 & \boldsymbol{M}_{IB} \end{bmatrix} \tag{19}$$

Regarding the orthogonality of the rotation matrix ${}^{w}\boldsymbol{R}_B$ i.e., ${}^{w}\boldsymbol{R}_B{}^{-1} \equiv {}^{w}\boldsymbol{R}_B{}^{T}$, $I_{Bxx} \neq 0$, $I_{Byy} \neq 0$ and $I_{Bzz} \neq 0$. Thus, the entire system could be reduced to a fully actuated system with 6 inputs and 6 outputs (i.e., generalized coordinate variables). The input thrust $\boldsymbol{f}^B$ and input torque $\boldsymbol{\tau}_{input}$ are determined by:

$$\begin{bmatrix} f^B \\ \tau_{input} \end{bmatrix} \triangleq \begin{bmatrix} -2k_f a_1 + 2k_f a_2 \\ 2k_f a_3 - 2k_f a_4 \\ -2k_f a_5 - 2k_f a_6 \\ -2hk_f a3 + 2hk_f a4 \\ 2lk_f a_5 - 2lk_f a_6 - 2hk_f a_1 + 2hk_f a_2 \\ 2lk_f a_3 - 2lk_f a_4 \end{bmatrix} \tag{20}$$

In which $a_1 = cos\alpha_1 sin\beta_1 \omega_1^2, a_2 = cos\alpha_2 sin\beta_2 \omega_2^2,$
$a_3 = sin\alpha_1 \omega_1^2, a_4 = sin\alpha_2 \omega_2^2, a_5 = cos\alpha_1 cos\beta_1 \omega_1^2$ *and* $a_6 = cos\alpha_2 cos\beta_2 \omega_2^2$

6 Backstepping Control Method

The backstepping control was used in most of the trajectory tracking control literature [53]. In this regard, a MIMO vectorial backstepping approach as described in this section:

6.1 Derivation about the First Lyapunov Function

Start by introducing a state variable representation,

$$\boldsymbol{x}_1 = \boldsymbol{X}, \boldsymbol{x}_2 = \dot{\boldsymbol{X}} \tag{21}$$

Equation (16) can be written as:

$$\begin{aligned} \dot{\boldsymbol{x}}_1 &= \boldsymbol{x}_2 \\ \dot{\boldsymbol{x}}_2 &= \boldsymbol{f}(\boldsymbol{x}_2) + \boldsymbol{g}(\boldsymbol{x}_1)(\boldsymbol{U} + \boldsymbol{w}) \end{aligned} \tag{22}$$

Taking the position error as $\boldsymbol{e}_1 = \boldsymbol{x}_{1d} - x_1$, where x_{1d} shows the desired reference trajectory, the first Lyapunov function is selected as:

$$\boldsymbol{V}_1 = \frac{1}{2}\boldsymbol{e}_1^T \boldsymbol{e}_1 \tag{23}$$

The derivative of $\boldsymbol{V}_1$ with respect to time will be:

$$\dot{\boldsymbol{V}}_1 = \boldsymbol{e}_1^T \dot{\boldsymbol{e}}_1 = \boldsymbol{e}_1^T (\dot{\boldsymbol{x}}_{1d} - \dot{\boldsymbol{x}}_1) \tag{24}$$

A stabilizing function is designed to stabilize $\boldsymbol{e}_1$:

$$\boldsymbol{\alpha}_1 = \dot{\boldsymbol{x}}_{1d} + \boldsymbol{K}_1 \boldsymbol{e}_1 \tag{25}$$

where $\boldsymbol{K}_1 > 0$. Substituting $\dot{\boldsymbol{x}}_{1d}$ in $\dot{\boldsymbol{V}}_1$ by (25), $\dot{\boldsymbol{V}}_1$ can be obtained as:

$$\begin{aligned} \dot{\boldsymbol{V}}_1 &= \boldsymbol{e}_1^T (-\boldsymbol{K}_1 \boldsymbol{e}_1 + \boldsymbol{\alpha}_1 - \dot{\boldsymbol{x}}_1) \\ &= \boldsymbol{e}_1^T (-\boldsymbol{K}_1 \boldsymbol{e}_1 + \boldsymbol{\alpha}_1 - \boldsymbol{x}_2) \\ &= -\boldsymbol{e}_1^T \boldsymbol{K}_1 \boldsymbol{e}_1 + \boldsymbol{e}_1^T \boldsymbol{e}_2 \end{aligned} \tag{26}$$

where $\boldsymbol{e}_2 = \boldsymbol{\alpha}_1 - \boldsymbol{x}_2$ shows an extended velocity tracking error. When $\boldsymbol{e}_2 \equiv \boldsymbol{0}, \dot{\boldsymbol{V}}_1 = -\boldsymbol{e}_1^T \boldsymbol{K}_1 \boldsymbol{e}_1 \leq \boldsymbol{0}$ can be determined.

6.2 Derivation about the Second Lyapunov Function

Considering the following velocity error:

$$\boldsymbol{e}_2 = \boldsymbol{\alpha}_1 - \boldsymbol{x}_2 = \dot{\boldsymbol{x}}_{1d} - \dot{\boldsymbol{x}}_1 + \boldsymbol{K}_1 \boldsymbol{e}_1 \tag{27}$$

the derivative of e_2 will be:

$$\begin{aligned} \dot{\boldsymbol{e}}_2 &= \dot{\boldsymbol{\alpha}}_1 - \dot{\boldsymbol{x}}_2 \\ &= \ddot{\boldsymbol{x}}_{1d} + \boldsymbol{K}_1 \dot{\boldsymbol{e}}_1 - \boldsymbol{f}(\boldsymbol{x}_2) - \boldsymbol{g}(\boldsymbol{x}_1)(\boldsymbol{U} + \boldsymbol{w}) \end{aligned} \tag{28}$$

The second Lyapunov function can be expressed by:

$$\boldsymbol{V}_2 = \boldsymbol{V}_1 + \frac{1}{2}\boldsymbol{e}_2^T \boldsymbol{e}_2 \equiv \frac{1}{2}\boldsymbol{e}_1^T \boldsymbol{e}_1 + \frac{1}{2}\boldsymbol{e}_2^T \boldsymbol{e}_2 \tag{29}$$

Then the derivative of $\boldsymbol{V}_2$ with respect to time is:

$$\dot{\boldsymbol{V}}_2 = \dot{\boldsymbol{V}}_1 + \boldsymbol{e}_2^T \dot{\boldsymbol{e}}_2 \tag{30}$$

Combining the Eqs. (23) and (25), $\dot{\boldsymbol{V}}_2$ will result in:

$$\dot{\boldsymbol{V}}_2 = -\boldsymbol{e}_1^T \boldsymbol{K}_1 \boldsymbol{e}_1 + \boldsymbol{e}_1^T \boldsymbol{e}_2 + \boldsymbol{e}_2^T \begin{bmatrix} \ddot{\boldsymbol{x}}_{1d} + \boldsymbol{K}_1 \dot{\boldsymbol{e}}_1 - \boldsymbol{f}(\boldsymbol{x}_2) - \\ \boldsymbol{g}(\boldsymbol{x}_1)(\boldsymbol{U} + \boldsymbol{w}) \end{bmatrix} \tag{31}$$

For stabilizing e_2, the control input $\boldsymbol{U}$ can be written by:

$$\boldsymbol{U} = \boldsymbol{g}^{-1}(\boldsymbol{x}_1)\left[\boldsymbol{K}_2 \boldsymbol{e}_2 + \ddot{\boldsymbol{x}}_{1d} + \boldsymbol{K}_1 \dot{\boldsymbol{e}}_1 - \boldsymbol{f}(\boldsymbol{x}_2) - \boldsymbol{g}(\boldsymbol{x}_1)\boldsymbol{w} + \boldsymbol{e}_1\right] \tag{32}$$

where $\boldsymbol{K}_2 > 0$ and $\boldsymbol{g}^{-1}(\boldsymbol{x}_1)$ is known. Substituting (32) to (31), therefore $\dot{\boldsymbol{V}}_2 = -\boldsymbol{e}_1^T \boldsymbol{K}_1 \boldsymbol{e}_1 - \boldsymbol{e}_2^T \boldsymbol{K}_2 \boldsymbol{e}_2 \leq \boldsymbol{0}$. $\boldsymbol{e}_1$ and $\boldsymbol{e}_2$ will converge to zero when $t \to \infty$, such a controlled system guarantees asymptotic stability. The block diagram of the proposed backstepping control method is presented in Fig. 15.

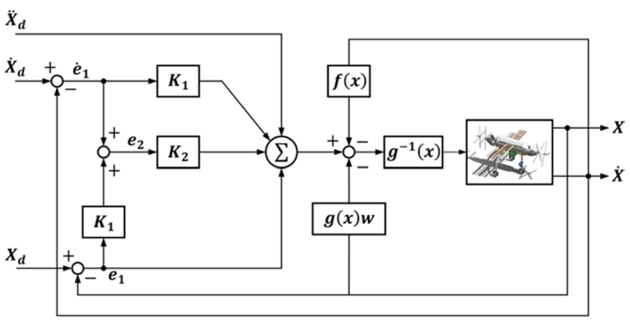

Fig. 15 The overall control block diagram

6.3 Simulation Results

An example (Asymptotic Trajectory Tracking) was simulated by MATLAB for verification of the developed backstepping control approach. The following physical parameters of the MICOPTER were considered in the simulation: $m = 17$ kg, $g = 9.81\ m/s^2$, $l = 0.4$ m, $h = 0.15$ m and, $k_f = 7.19 \times 10^{-6} N/(rpm)^2$. The control gains were $K11 = K12 = K13 = 1$, $K14 = K15 = K16 = 2$, and $K21 = K22 = K23 = K24 = K25 = K26 = 1$. The sampling width of the simulations is also taken 0.01 s.

In the trajectory tracking simulation, a 3D space trajectory was set to $\boldsymbol{X_d}(t) = [xd(t) yd(t) zd(t) \frac{\pi}{6}\ \frac{\pi}{6}\ \frac{\pi}{6}]^T$ while the initial state of the system was adjusted to $\boldsymbol{X}_0 = [000000]^T$, where the trajectory can be defined as:

$$\begin{cases} x_d(t) = 0.5 * \sin\left(\frac{\pi}{4}t\right) \\ y_d(t) = -0.5 * \cos\left(\frac{\pi}{8}t\right) \\ z_d = 1 \end{cases} \tag{33}$$

where t represents the time. The position responses of the MICOPTER in the trajectory simulation are depicted in Fig. 16. According to Fig. 17, the attitude responses of the MICOPTER converged to the desired levels.

Additionally, Fig. 18 illustrates the trajectory in three-dimensional space with negligible errors between the desired and current trajectories. The simulation confirms the effectiveness of the developed backstepping control strategy in terms of the position and attitude controls. The MICOPTER showed a stable flight while its body was maintained in the desired attitude during the simulation.

7 Conclusions

In this paper, a new concept of a hybrid drone called "MICOPTER" using the Bi-copter approach was introduced in the conceptual design phase. Then, multi-objective multidisciplinary design optimization of MICOPTER was performed to maximize both cruise velocity and range as objectives and results proposed as the Pareto frontier. The feasible design points in the Pareto frontiers confirmed that the MICOPTER could fulfill the mission goals as well as the ability to carry payloads from 2 to 6 kg in a wide bound of velocity and range with minimum changes in the configuration. Eventually, the equations of the motion were extracted, and a typical flight profile, using a robust non-linear backstepping control, was simulated. The performance of the controller was assessed considering its stability and tracking 8-shape trajectory for one of the selected optimal design points.

Future research topic suggestions include extensions of the problem to high fidelity analysis modules, detailed design, and considering higher dimensions of design variables and uncertainties. To alleviate the computational burden of such problems using surrogate-assisted design optimization will be beneficial. Control and simulation of Hover-Cruise

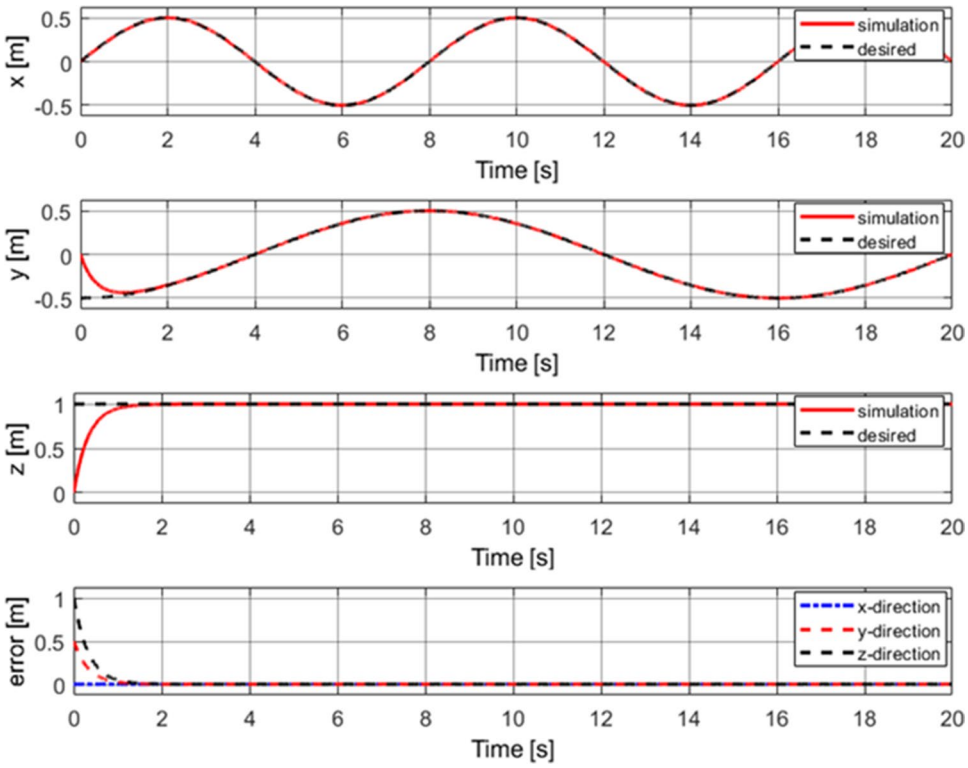

Fig. 16 Responses to position control in trajectory tracking

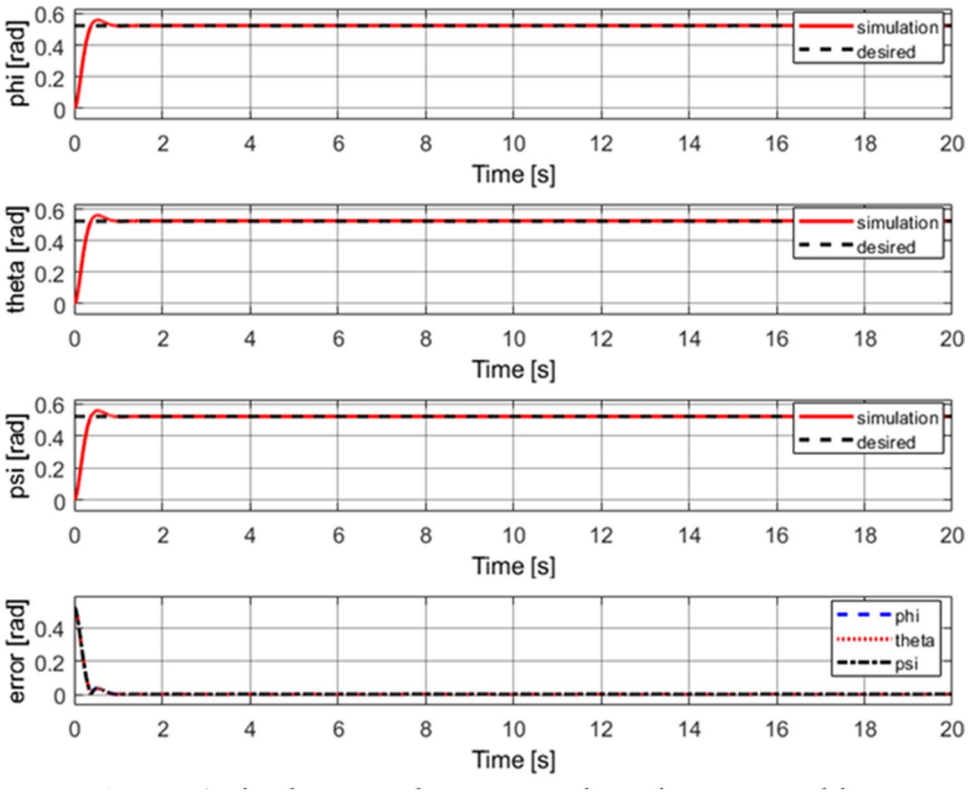

Fig. 17 Attitude control responses in trajectory tracking

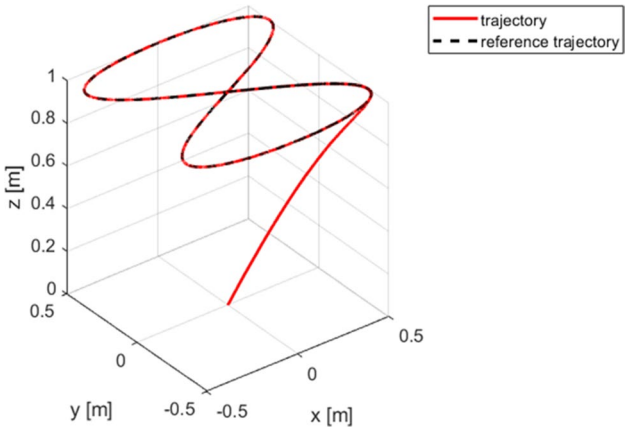

Fig. 18 The MICOPTER 8-shape trajectory tracking

transition phase is another step to be taken. Finally, by passing various hardware-in-loop tests and system identifications, a prototype will be built for the flight test.

Author Contributions Arian Abedini, Ali Asghar Bataleblu and Jafar Roshanian, made this manuscript and did the research.

Data Availability Not Applicable.

Declarations

Ethical Approval This paper does not report research that requires ethical approval. Consent to participate or consent to publish statements are accordingly also not required.

Consent to Participate All authors have read and agreed to publish this work.

Consent for Publication All authors have read and agreed to publish this work.

Conflicts of Interest On behalf of all authors, the corresponding author states that there is no conflict of interest.

References

1. Chamola, V., Hassija, V., Gupta, V., Guizani, M.: A comprehensive review of the COVID-19 pandemic and the role of IoT, drones, AI, blockchain, and 5G in managing its impact. IEEE Access. **8**, 90225–90265 (2020)
2. Darvishpoor, S., Roshanian, J., Raissi, A., Hassanalian, M.: Configurations, flight mechanisms, and applications of unmanned aerial systems: a review. Prog. Aerosp. Sci. **121**, 100694 (2020)
3. Ducard, G.J., Allenspach, M.: Review of designs and flight control techniques of hybrid and convertible VTOL UAVs. Aerosp. Sci. Technol. **118**, 107035 (2021)
4. Yuan, C., Liu, Z., Zhang, Y.: Learning-based smoke detection for unmanned aerial vehicles applied to forest fire surveillance. J. Intell. Rob. Syst. **93**(1), 337–349 (2019)
5. Saeed, A.S., Younes, A.B., Cai, C., Cai, G.: A survey of hybrid unmanned aerial vehicles. Prog. Aerosp. Sci. **98**, 91–105 (2018)
6. Bell Eagle Eye. Wikipedia. https://en.wikipedia.org/wiki/Bell_Eagle_Eye (2017). Accessed 22 Jan 2022
7. Van Duijn, L.: DHL Parcelcopter 3. VMware. https://vdr.one/dhl-parcelcopter-3/ (2016). Accessed 22 Jan 2022
8. Low, J.E., Win, L.T.S., Shaiful, D.S.B., Tan, C.H., Soh, G.S., Foong, S.: Design and dynamic analysis of a transformable

hovering rotorcraft (thor). IEEE International Conference on Robotics and Automation (ICRA), pp. 6389–6396 (2017)
9. Rees, C.: Arcturus JUMP™15 Fixed Wing VTOL UAV. Unmanned Systems Technology. https://www.unmannedsystemstechnology.com/video/arcturus-jump15-fixed-wing-vtol-uav/ (2015). Accessed 22 Jan 2022
10. Xu, J.: Design perspectives on delivery drones. RAND London (2017)
11. Wingcopter. spec sheet. https://wingcopter.com/wp-content/uploads/2021/02/Technical-Details-Wingcopter-178-Heavy-Lift-A-Delivery-Variant-1-1.pdf (2010). Accessed 22 Jan 2022
12. Coxworth, B.: DHL Parcelcopter takes to Tanzanian skies. Newatlas. https://newatlas.com/dhl-parcelcopter-africa/56663/ (2018). Accessed 22 Jan 2022
13. Wingcopter. https://wingcopter.com/wingcopter-198#specs (2020). Accessed 22 Jan 2022
14. GH Craft. QTW-UAS FS4 spec sheet. https://ghcraft.com/QTW/pdf/081001_QTW_FS4e.pdf (2009). Accessed 22 Jan 2022
15. Holsten, J., Ostermann, T., Moormann, D.: Design and wind tunnel tests of a tiltwing UAV. CEAS Aeronaut. J. **2**(1), 69–79 (2011)
16. Amazon. https://www.amazon.com/Amazon-Prime-Air/b?ie=UTF8&node=8037720011 (2016). Accessed 22 Jan 2022
17. Rahimi, F.: Multi-Criteria Co-Design optimization of Mechatronic Systems. In 2020 IEEE International Conference on Mechatronics and Automation (ICMA), pp. 756–766 (2020)
18. Palmer, A.: Amazon wins FAA approval for Prime Air drone delivery fleet. CNBC. https://www.cnbc.com/2020/08/31/amazon-prime-now-drone-delivery-fleet-gets-faa-approval.html (2020). Accessed 22 Jan 2022
19. Baldwin, G.: Rapid Vertical Deployment Systems .Baldwin Technology Company. https://baldwintech.com/ (2005). Accessed 22 Jan 2022
20. Zeng, L., Hu, J., Pan, D., Shao, X.: Automated design optimization of a mono tiltrotor in hovering and cruising states. Energies **13**(5), 1155 (2020)
21. Leishman, J.G.: Aerodynamic optimization of a coaxial proprotor. In: The American Helicopter Society 62nd Annual Forum (2006)
22. Rand, O., Khromov, V.: Aerodynamic optimization of coaxial rotor in hover and axial flight. In: 27th international Congress of the Aeronautical Sciences, pp. 1–13 (2010)
23. Zhang, H., Song, B., Li, F., Xuan, J.: Multidisciplinary design optimization of an electric propulsion system of a hybrid UAV considering wind disturbance rejection capability in the quadrotor mode. Aerosp. Sci. Technol. **110**, 106372 (2021)
24. Gu, H., Lyu, X., Li, Z., Zhang, F.: Coordinate descent optimization for winged-UAV design. J. Intell. Rob. Syst. **97**(1), 109–124 (2020)
25. Bin Junaid, A., Diaz De Cerio Sanchez, A., Betancor Bosch, J., Vitzilaios, N., Zweiri, Y.: Design and implementation of a dual-axis tilting quadcopter. Robotics. **7**(4), 65 (2018)
26. Jeong, J., Yoon, S., Kim, S. K., Suk, J.: Dynamic modeling and analysis of a single tilt-wing unmanned aerial vehicle. In: AIAA Modeling and Simulation Technologies Conference, pp. 1804 (2015)
27. Yan, X., Chen, R., Lou, B., Xie, Y., Xie, A., Zhang, D.: Study on control strategy for tilt-rotor aircraft conversion procedure. J. Phys.: Conf. Ser. **1924**(1), 012010 (2021)
28. Chen, Z., Jia, H.: Design of flight control system for a novel tilt-rotor UAV. Complexity (2020)
29. Djordjevic, V., Stojanovic, V., Tao, H., Song, X., He, S., Gao, W.: Data-driven control of hydraulic servo actuator based on adaptive dynamic programming. Discrete Cont. Dyn. Syst.-S. **15**(7), 1633 (2022)
30. Jiang, Y., Gao, W., Na, J., Zhang, D., Hämäläinen, T.T., Stojanovic, V., Lewis, F.L.: Value iteration and adaptive optimal output regulation with assured convergence rate. Control. Eng. Pract. **121**, 105042 (2022)
31. Zhuang, Z., Tao, H., Chen, Y., Stojanovic, V., Paszke, W.: Iterative learning control for repetitive tasks with randomly varying trial lengths using successive projection. Int. J. Adapt. Control Signal Process. **36**(5), 1196–1215 (2022)
32. Abedini, A., Bataleblu, A.A., Roshanian, J.: Robust backstepping control of position and attitude for a Bi-copter drone. In: 2021 9th RSI International Conference on Robotics and Mechatronics (ICRoM), pp. 425–432 (2021)
33. Jo, D., Kwon, Y.: Analysis of VTOL UAV propellant technology. J. Comput. Commun. **5**(7), 76–82 (2017)
34. Khudair, O.A., Aziz, S.A., Munshid, H.A., Rzokhy, H.M., Fared, S.: Improvement of micro UAV performance using tandem-wing design. Al-Nahrain J. Eng. Sci. **19**(2), 363–369 (2016)
35. Kim, H.W., Brown, R.E.: A comparison of coaxial and conventional rotor performance. J. Am. Helicopter Soc. **55**(1), 12004–12004 (2010)
36. Imam, A., Bicker, R.: Design and construction of a small-scale rotorcraft uav system. Int. J. Eng. Sci. Innov. Technol. **2** (2014)
37. Kamal, A.M., Ramirez-Serrano, A.: Design methodology for hybrid (VTOL+ Fixed Wing) unmanned aerial vehicles. Aeronaut. Aerosp. Open Access J. **2**(3), 165–176 (2018)
38. Silva, H.L., Resende, G.J., Neto, R., Carvalho, A.R., Gil, A.A., Cruz, M.A., Guimarães, T.A.: A multidisciplinary design optimization for conceptual design of hybrid-electric aircraft. Struct. Multidiscip. Optim. **64**(6), 3505–3526 (2021)
39. Balesdent, M., Bérend, N., Dépincé, P., Chriette, A.: A survey of multidisciplinary design optimization methods in launch vehicle design. Struct. Multidiscip. Optim. **45**(5), 619–642 (2012)
40. McDonald, R.A.: Advanced modeling in OpenVSP. In: 16th AIAA Aviation Technology, Integration, and Operations Conference, pp. 3282 (2016)
41. McDonald, R.A., Gloudemans, J.R.: Open vehicle sketch pad: an open source parametric geometry and analysis tool for conceptual aircraft design. In: AIAA SCITECH 2022 Forum. 0004 (2022)
42. Quitter, J.W., Marino, M., Bauschat, J.M.: Comparison of aerodynamic methods for flight mechanical derivative estimation of unconventional aircraft. In AIAA Scitech 2021 Forum. pp. 0324 (2021)
43. Marien, F.: Software Testing: VSPAERO. Master's thesis, Aircraft Design and Systems Group (AERO), Department of Automotive and Aeronautical Engineering, Hamburg University of Applied Sciences (2021)
44. Karakas, H., Koyuncu, E., Inalhan, G.: ITU tailless UAV design. J. Intell. Rob. Syst. **69**(1), 131–146 (2013)
45. Wu, X.: Design and Development of Variable Pitch Quadcopter for Long Endurance Flight. Doctoral dissertation, Oklahoma State University (2018)
46. Drela, M., Youngren, H.: Qprop. Massachusetts Institute of Technology. http://web.mit.edu/drela/Public/web/qprop/ (2008). Accessed 22 Jan 2022
47. Gövˇ, İ: Rotor spacing and blade number effect on the thrust, torque and power of a coaxial rotor. El-Cezeri J. Sci. Eng. **7**(2), 487–502 (2020)
48. Khofiyah, N.A., Sutopo, W., Nugroho, B.D.A.: Technical feasibility battery lithium to support unmanned aerial vehicle (UAV): a technical review. In Proceedings of the International Conference on Industrial Engineering and Operations Management, pp. 3591–3601 (2019)
49. Kamal, A., Ramirez-Serrano, A.: Systematic approach to conceptual design selection for hybrid UAVs using structured design methods. In: AIAA Scitech 2019 Forum, pp. 2097 (2019)
50. Mahmud, M.S.A., Abidin, M.S.Z., Buyamin, S., Emmanuel, A.A., Hasan, H.S.: Multi-objective route planning for underwater cleaning robot in water reservoir tank. J. Intell. Rob. Syst. **101**(1), 1–16 (2021)
51. Gudmundsson, S.: General Aviation Aircraft Design: Applied Methods and Procedures. Butterworth-Heinemann (2013)
52. Xu, X., Watanabe, K., Nagai, I.: Backstepping control for a tandem rotor UAV Robot with two 2-DOF tiltable coaxial rotors. J. Robot. Control **2**(5), 413–420 (2021)
53. Rubí, B., Pérez, R., Morcego, B.: A survey of path following control strategies for UAVs focused on quadrotors. J. Intell. Rob. Syst. **98**(2), 241–265 (2020)

Arian Abedini received the B.S. degree in mechanical engineering from the Sirjan University of Technology, Kerman, Iran, in 2019 and M.S. degree in Aerospace Engineering-Flight Dynamics and Control from K.N.Toosi University of Technology, Tehran, Iran, in 2022. His research interests include Co-Design and Co-simulation of control systems, Intelligent and Nonlinear control and implementing for different type of drones, Drones Design and construction, Robotics system design, Systems identification of robots, Hardware and software in the loop simulation, Modeling and Simulation of Complicated Dynamic Systems.

Ali Asghar Bataleblu received his M.Sc. and Ph.D. degrees in Aerospace Engineering from KNTU in 2012 and 2018 respectively. He has more than ten years of work experience in the Space System Design Institute (SSDI) at KNTU from disciplinary analyses to systems engineer. His research specifically focused on systems engineering and MBSE, uncertainty-based MDO, flight dynamic and control, machine learning, co-simulation, and co-design. The application areas for his research have included mechanical and aerospace engineering and robotics.

Jafar Roshanian received the M.S. and Ph.D. degree in Aerospace Engineering-Flight Dynamics and Control from Moscow State Technical University, Russia, in 1996 and 1999 respectively. He is currently a full professor in the Department of Aerospace Engineering at the K.N. Toosi University of Technology, Tehran, Iran. His research interests include Design and Simulation of Space Trajectory, Multidisciplinary Design Optimization (MDO), Guidance Algorithms and Attitude Control Systems, Adaptation Theory with Application to Flight Control Systems and Celestial attitude and position determination.